

## Numerical Analysis of Seepage in Steady and Transient Flow State by the Radial Basis Function Method

Rasoul Daneshfaraz<sup>\*</sup>, Sina Sadeghfam<sup>\*\*</sup>, Roghayeh Adami<sup>\*\*\*</sup>, Hamidreza Abbaszadeh<sup>\*\*\*\*</sup>

### ARTICLE INFO

#### RESEARCH PAPER

#### Article history:

Received:  
March 2023.

Revised:  
July 2023.

Accepted:  
August 2023.

#### Keywords:

Meshless Method,  
Finite Element Method,  
Steady Flow,  
Transient Flow,  
Seepage

### Abstract:

Here, the meshless method with the finite difference method has been used to discretize the governing equations of the seepage phenomenon from under the dam in the steady and transient flow. The seepage problem was solved by considering the 6656 triangular mesh and 3449 nodes by the Finite Element Method and was used for validation. The radial basis function method (RBF) was considered one of the methodological methods to solve the seepage problem by considering several points. The results showed that by increasing the number of points, the accuracy of the solution increases, and the error decreases. The results of statistical indicators in the RBF method are reduced compared to the Finite Element Method. The results showed the proximity of the initial approximations to the original answer. The shape factor of the base function depends on the geometry and the governing equation, so the exact shape factor was used for the steady and transient state. In the transient condition, with the water level behind the dam remaining constant, the water head below the dam also reaches a constant value over time. The calculation of statistical indicators showed that the solution by the RBF method has acceptable accuracy.

## 1. Introduction

Solving the equation governing the phenomenon of seepage is one of the most proposed and complex problems in hydraulics, and various numerical methods to solve this equation, such as the Finite Difference Method [1], Finite Element Method [2], Boundary Element Method [3] and Finite Volume Method [4] presented. The common feature of these methods is that the solution area and boundaries must be networked first, and the problem-solving operation is done through networking. The results obtained in these methods are highly dependent on the mesh and related computational networks [5-7]. This factor prevents using these methods in two or three-dimensional problems or

nonlinear engineering problems with a complex and irregular study area. In recent years, the development of the meshless method has eliminated the weakness of mesh dependence. In this method, numerical approximations for solving differential equations are performed not based on elements and the relationships between them but based on a set of points. The primary purpose of meshless methods is to remove part of the traditional structure in mesh-dependent methods. The main idea of meshless methods is to approximate the whole field of the problem with only points. Different meshless methods have been developed, each with advantages and disadvantages. Among the various methods, the radial basis functions method is more prevalent among researchers due to its univariate nature. Among the reasons for the popularity of the RBF meshless method are the following [8]:

- 1- There is no need to discretize the solution area or boundaries.
- 2- Overlap of the solution area or boundaries is not required.
- 3- In some problems, convergence has a high speed.

\* Corresponding author: Professor, Department of Civil Engineering, Faculty of Engineering, University of Maragheh, Maragheh, Iran.  
Email: [daneshfaraz@maragheh.ac.ir](mailto:daneshfaraz@maragheh.ac.ir)

\*\* Assistant Professor, Department of Civil Engineering, Faculty of Engineering, University of Maragheh, Maragheh, Iran.

\*\*\* M.sc student Department of Civil Engineering, Faculty of Engineering, University of Maragheh, Maragheh, Iran.

\*\*\*\* M.sc student, Department of Civil Engineering, Faculty of Engineering, University of Maragheh, Maragheh, Iran.

4. Since RBF univariate functions depend only on the distances between points, it is suitable for solving multidimensional problems, and additional information, such as internal conditions, can be reduced (or added) at each modeling step.

5. The coding of meshless methods is relatively simple compared to other methods.

6- Compared to other methods, the answer is faster.

The basic idea of meshless methods in solving problems related to astrophysics by Gingold and Monaghan [9] is that the discretization of equations does not have boundary conditions due to the infinity of the solution region. The first time, Kansa [10] used the Multi Quadratic (MQ) approximation to solve elliptic, parabolic, and hyperbolic equations. Boztosun, et al. [11] solved the advection-diffusion equation using the RBF Collection Method (RBFCM) and compared the results with the Finite Difference Method. This study showed that the RBF method responds faster than the Finite Difference Method. Sarler, et al. [12] solved the Darcy natural convection problem under porous conditions using the RBFCM method, compared the results with the results of the Finite Volume Method, and observed a good agreement between the two methods. Durmus et al. [13] used the meshless method with the radial basis function to solve the transfer-diffusion equation and reported the excellent agreement of the results of this method with the results of the Boundary Element and Finite Difference Methods. Nourani and Mousavi [14] modeled the groundwater level by combining the two methods of artificial intelligence, ANN and ANFIS, and the meshless method. Their research showed that the RBF-ANFIS method gives more accurate results than the RBF-ANN method. Hashemi and Hatam [15] used the RBF method based on the Quadratic Differential method (RBF-DQ) to analyze the non-continuous seepage under the dam and compared the results with other methods, such as the finite element method. Their results showed that the solution by the RBF-DQ method is more accurate.

The present study investigates seepage from under the dam using the RBF meshless numerical method. Hashemi and Hatam [15] and Ouria et al. [16] research data have been used for the solution in this study. A review of previous research showed that, so far, no study has been done on seepage under the dam using the RBF meshless method in the steady flow state. The results were validated by the Finite Element Method and Local BF-DQ method. Also, the shape factor is one of the most critical parameters in the RBF meshless method. This study introduces the appropriate shape factor for the seepage problem for the number of different points. Also, the effect of density and the number of points on the accuracy of solving the problem was investigated. The selection of the appropriate base function in the RBF meshless method is closely related to the quality

of problem-solving. Therefore, different base functions were considered as the base function in the RBF method, and the most appropriate function was introduced to describe the seepage phenomenon. In the present study, the goal is to numerically solve the steady and transient flow state equation or the Laplace equation, which uses the integration of the RBF meshless method and the Forward Finite Difference for spatio-temporal modeling of the seepage phenomenon under the dam. Another goal of this study is to draw the equipotential lines under the dam using the minimum points and with appropriate accuracy with the meshless method.

## 2. Materials and Methods

Richards first proposed the partial differential equation of water motion in a porous environment by combining the two equations of continuity and Darcy. The Richards equation for the two-dimensional state is in the form of Equation 1 [17]:

$$\frac{\partial}{\partial x} \left( k_r k_x \frac{\partial h}{\partial x} \right) + \frac{\partial}{\partial y} \left( k_r k_y \frac{\partial h}{\partial y} \right) = \left( S_w S_s + n \frac{dS_w}{dp} \right) \frac{dh}{dt} \quad (1)$$

Where  $x$  and  $y$  are horizontal and vertical directions, respectively,  $k_x$  and  $k_y$  are hydraulic conductivity in the direction of  $x$  and  $y$ , respectively,  $k_r$  is the relative permeability (in the saturation zone is equal to one),  $S_w$  is the water saturation ratio,  $S_s$  is the special maintenance,  $n$  is the porosity,  $h$  is the hydraulic head, and  $p$  is the pressure head. For saturated regions, the amount of hydraulic conductivity is considered constant in two directions, so Equation 1 can be written as Equation 2 [18]:

$$k_x \frac{\partial^2 h}{\partial x^2} + k_y \frac{\partial^2 h}{\partial y^2} = S_s \frac{\partial h}{\partial t} \quad (2)$$

Considering homogeneous and homologous soils ( $k_x = k_y$ ), Equation 2 can be rewritten as Equation 3 [19]:

$$\frac{\partial^2 h}{\partial x^2} + \frac{\partial^2 h}{\partial y^2} = \frac{S_s}{k} \frac{\partial h}{\partial t} \quad (3)$$

For the steady flow, Equation 3 is written as Equation 4, which is the same as Laplace Equation [19]:

$$\frac{\partial^2 h}{\partial x^2} + \frac{\partial^2 h}{\partial y^2} = 0 \Rightarrow \nabla^2 h = 0 \quad (4)$$

RBFs are univariate functions that are suitable for solving complex and multidimensional problems. In solving the

problem by RBF method, Equation 5 is established in the computational area with internal points  $\Omega$  and boundary points  $\partial\Omega$ :

$$Lh = f \quad \text{in } \Omega \tag{5}$$

$$Bh = g \quad \text{in } \partial\Omega$$

B and L are the differential operators at the interior and boundary points of the computational area, respectively. The approximate solution of Equation 5 in the RBF mesh method can be estimated as Equation 6:

$$h = \sum_{i=1}^N c_i \varphi_i(r) \tag{6}$$

Where  $\varphi_i$  is the radial basis function or shape function that is always a function of the distance between points,  $c_i$  unknown coefficients,  $N$  is the total number of nodes (some on the border and some inside the solution area) that are optionally and randomly selected from the computational area without mesh creating.

Important basic functions used in the RBF meshless method include Multi-Quadratic, Gaussian, Poly-harmonic, Conical, Inverse multi-quadratic, and Inverse quadratic. These shape functions are shown in Equations 7 to 12, respectively.

$$\varphi_{(r)} = (r^2 + \alpha^2)^{\beta/2} \tag{7}$$

$$\varphi_{(r)} = e^{-\alpha r^2} \tag{8}$$

$$\varphi_{(r)} = r^n \log r \tag{9}$$

$$\varphi_{(r)} = r^n \tag{10}$$

$$\varphi_{(r)} = \left( 1 / (r^2 + \alpha^2)^{\beta/2} \right) \tag{11}$$

$$\varphi_{(r)} = \left( 1 / (r^2 + \alpha^2) \right) \tag{12}$$

In the above functions,  $r$  is the distance between points,  $\alpha$ ,  $\beta$ , and  $n$  are the values obtained by calibration. In the Conical function, the value of  $\alpha$  should be considered a natural odd number, and in the Poly-harmonic function, the value of  $\alpha$  should be considered a natural even number. Any real number can be taken in the Multi Quadratic function for  $\alpha$ . For calibration, different values for  $\alpha$ ,  $\beta$ , and  $n$  are considered, then the problem is solved with those values, and the result obtained is validated by analytical or laboratory results or the result of a valid numerical method, and the error value is calculated. The value for which the error decreases is the optimal value for  $\alpha$ ,  $\beta$ , and  $n$ .

This study applies the head and its specific gravity while defining the upstream initial conditions. Also, in defining the boundary conditions for the areas through which water does not pass, the closed flow boundary condition is defined in the software.

In the present study, the MQ function is used to solve the equation governing the seepage phenomenon, and then the correctness of this function will be checked and proved. Assuming  $\beta=1$  in the Multi Quadratic (MQ) base function to analyze seepage under a concrete dam for a two-dimensional state, Equation 13 can be written:

$$h(x, y) = \sum_{j=1}^N c_j \sqrt{(x - x_j)^2 + (y - y_j)^2 + \alpha^2} \tag{13}$$

Equation 13 is written for all points on the boundaries and inside the computational area to solve the problem by the RBF method. Therefore, the number of points considered on the boundaries and inside the computational area, equation, and unknown are obtained. By solving in matrix form, a matrix for  $c$  will be obtained. Therefore, solving the problem involves calibrating the optimal  $\alpha$  (shape factor) and finding the corresponding matrix  $c$  with the optimal  $\alpha$ . The following schematics were considered (Figure 1) to explain the governing equations in the computational area and boundaries:

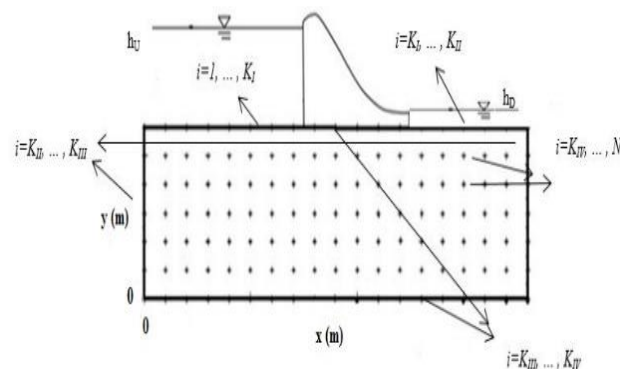


Fig. 1: Schematic diagram of computational area and boundary and internal points

In Figure 1, the expressions marked on the computational area of the boundary and internal points are  $h_U$  and  $h_D$ , respectively: water head upstream and downstream of the concrete dam,  $i = 1, \dots, K_I$ : number of points on the Dirichlet boundary with the value of the head  $h_U$ ,  $I = K_I, \dots, K_J$ : Number of points located on the Dirichlet boundary with the value of the head  $h_D$ ,  $i = K_K, \dots, K_M$ : Number of points located on the Newman boundary in the vertical direction,  $i = K_M, \dots, K_N$ : Number of points Located on the Newman boundary along the horizon and  $i = K_N, \dots, N$ : are the number of points located within the computational area.

Equations 3 and 4 govern the seepage phenomenon in transient and steady flow. By placing Equation 13 in Equation 4, Equation 14 is obtained:

$$\frac{\partial^2 \left( \sum_{j=1}^N c_j \sqrt{(x-x_j)^2 + (y-y_j)^2 + \alpha^2} \right)}{\partial x^2} + \frac{\partial^2 \left( \sum_{j=1}^N c_j \sqrt{(x-x_j)^2 + (y-y_j)^2 + \alpha^2} \right)}{\partial y^2} = 0 \quad (14)$$

The combination of the RBF meshless method and the Forward Finite Difference method is implicitly used to solve the problem in a transient flow state.

$$\frac{k}{S_s} \times \left( \frac{\partial^2 h}{\partial x^2} + \frac{\partial^2 h}{\partial y^2} \right)^{n+1} = \frac{h_i^{n+1} - h_i^n}{\Delta t} \quad (15)$$

$$\Delta t \times \frac{k}{S_s} \times \left( \frac{\partial^2 h}{\partial x^2} + \frac{\partial^2 h}{\partial y^2} \right)^{n+1} + h_i^n - h_i^{n+1} = 0$$

Equation 16 is obtained by placing Equation 13 in Equation 15.

$$\Delta t \times \frac{k}{S_s} \times \left( \frac{\partial^2 \left( \sum_{j=1}^N c_j \sqrt{(x-x_j)^2 + (y-y_j)^2 + \alpha^2} \right)}{\partial x^2} + \frac{\partial^2 \left( \sum_{j=1}^N c_j \sqrt{(x-x_j)^2 + (y-y_j)^2 + \alpha^2} \right)}{\partial y^2} \right)^{n+1} - \left( \sum_{j=1}^N c_j \sqrt{(x-x_j)^2 + (y-y_j)^2 + \alpha^2} \right)^{n+1} + \left( \sum_{j=1}^N c_j \sqrt{(x-x_j)^2 + (y-y_j)^2 + \alpha^2} \right)^n = 0 \quad (16)$$

For Newman boundaries in the vertical direction, the value of the variable vertical gradient, the water head, is zero, according to Equation 17.

$$\frac{\partial h}{\partial x} = 0 \quad (17)$$

Equation 18 is obtained by substituting Equation 13 in Equation 17:

$$\frac{\partial \left( \sum_{j=1}^N c_j \sqrt{(x-x_j)^2 + (y-y_j)^2 + \alpha^2} \right)}{\partial x} = 0 \quad (18)$$

For Newman boundaries along the horizon, the value of the vertical gradient of the variable, which is the water head, is zero, as in Equation 19.

$$\frac{\partial h}{\partial y} = 0 \quad (19)$$

By placing Equation 13 in Equation 19 for a point, Equation 20 is obtained.

$$\frac{\partial \left( \sum_{j=1}^N c_j \sqrt{(x-x_j)^2 + (y-y_j)^2 + \alpha^2} \right)}{\partial y} = 0 \quad (20)$$

For the Dirichlet boundaries, Equation 13 is equal to the water head upstream and downstream, respectively, according to Equations 21 and 22:

$$\sum_{j=1}^N c_j \sqrt{(x-x_j)^2 + (y-y_j)^2 + \alpha^2} = h_U \quad (21)$$

$$\sum_{j=1}^N c_j \sqrt{(x-x_j)^2 + (y-y_j)^2 + \alpha^2} = h_D \quad (22)$$

Equation 23 is obtained by combining equations to achieve the matrix form of equations.

	$\varphi$	$C$	$h$	
	$\left[ \begin{array}{ccc} \varphi_1(x_1) & \dots & \varphi_N(x_1) \\ \vdots & & \vdots \\ \varphi_1(x_{K_i}) & \dots & \varphi_N(x_{K_i}) \\ \varphi_1(x_{K_i+1}) & \dots & \varphi_N(x_{K_i+1}) \\ \vdots & & \vdots \\ \varphi_1(x_{K_n}) & \dots & \varphi_N(x_{K_n}) \\ \varphi_1(x_{K_n+1}) & \dots & \varphi_N(x_{K_n+1}) \\ \vdots & & \vdots \\ \varphi_1(x_{K_m}) & \dots & \varphi_N(x_{K_m}) \\ \varphi_1(x_{K_m+1}) & \dots & \varphi_N(x_{K_m+1}) \\ \vdots & & \vdots \\ \varphi_1(x_{K_N}) & \dots & \varphi_N(x_{K_N}) \\ \varphi_1(x_{K_N+1}) & \dots & \varphi_N(x_{K_N+1}) \\ \vdots & & \vdots \\ \varphi_1(x_N) & \dots & \varphi_N(x_N) \end{array} \right]$	$\left[ \begin{array}{c} c_1 \\ \vdots \\ c_{K_i} \\ c_{K_i+1} \\ \vdots \\ c_{K_n} \\ c_{K_n+1} \\ \vdots \\ c_{K_m} \\ c_{K_m+1} \\ \vdots \\ c_{K_N} \\ c_{K_N+1} \\ \vdots \\ c_N \end{array} \right]$	$\left[ \begin{array}{c} h_U \\ \vdots \\ h_U \\ h_D \\ \vdots \\ h_D \\ \vdots \\ 0 \\ 0 \\ \vdots \\ 0 \\ 0 \\ \vdots \\ 0 \end{array} \right]$	$=$
				(23)

By considering the different shape factors, different matrices of  $c$  are obtained. The results are validated for different shape factors ( $\alpha$ ) using a valid method. The factor of shape for which the error resulting from the validation is minimal is considered the optimal shape factor. After calibrating  $\alpha$  and obtaining the corresponding  $c$  matrix, the water head can be calculated at any point. To evaluate the results obtained using the RBF meshless method, the root mean square error (RMSE), the relative root mean square error (RRMSE), the determination coefficient ( $R^2$ ) and the absolute error (AE) with Equations 24, 25, 26, and 27 were used, respectively [20-23].

$$RMSE = \sqrt{\frac{\sum_1^n (h_{FEM} - h_{RBF})^2}{n}} \quad (24)$$

$$RRMSE = \sqrt{\frac{\sum_1^n \left(\frac{h_{FEM} - h_{RBF}}{h_{FEM}}\right)^2}{n}} \quad (25)$$

$$R^2 = 1 - \frac{\sum (h_{FEM} - h_{RBF})^2}{\sum h_{FEM}^2 - \sum h_{RBF}^2} \quad (26)$$

$$AE = |h_{FEM} - h_{RBF}| \quad (27)$$

In these relations,  $n$  is the number of data,  $h_{FEM}$  is the water head in the Finite Element Method, and  $h_{RBF}$  is the water head in the RBF meshless method.

### 3. Results and Discussions

Here, research data of Hashemi and Hatam [15] have been used to investigate the phenomenon of seepage under the dam. In the present study, the computational area is shown in Figure 2. The water head is 0.5 m upstream and then increases to 1.5 m with a uniform rate. The water head downstream is constant and equal to zero. The length of the calculation area is 3.6 meters, and its width is 1.2 meters. The values of hydraulic conductivity ( $k$ ), special maintenance ( $S_s$ ), and soil type are taken  $1.7 \times 10^{-4}$  m/s,  $0.00001 \text{ m}^{-1}$  and silt, respectively.

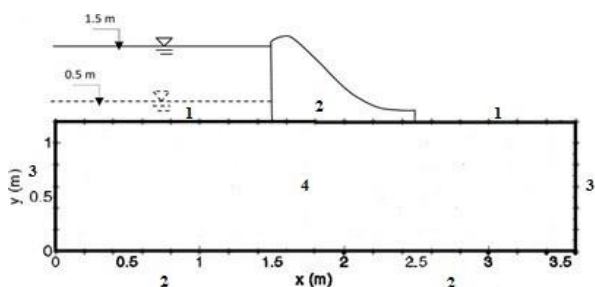


Fig. 2: Schematic diagram of the computational area of the seepage problem

In Figure 2, the boundaries of the solution area and the governing equations are as follows:

Boundaries No. 1: Permeable boundaries with Dirichlet boundary conditions with the condition  $h = h_U$  at upstream and  $h = h_D$  at downstream.

Boundaries No. 2: Impermeable boundaries with Newman boundary condition with condition  $\frac{\partial h}{\partial y} = 0$ .

Boundaries No. 3: Impermeable Boundaries with Newman boundary condition with condition  $\frac{\partial h}{\partial x} = 0$ .

Area No. 4: Within the computational area with relation  $\frac{\partial^2 h}{\partial x^2} + \frac{\partial^2 h}{\partial y^2} = \frac{\partial h}{\partial t}$ .

The results of the Finite Element Method with programming in MATLAB and Plaxis software were used to validate the RBF meshless method. Plaxis is an advanced finite element software used to analyze deformation and stability. This research considers the value of  $10 \text{ kN/m}^2$  for the specific water weight. A water head value is applied to the upstream slope to model water flow. A Closed flow boundary blocks areas where water does not pass. To calculate the flow, selecting the Water pressures option from the Generate menu will reveal the Water pressure generation window. In this window, information, including output flow rate, pore pressure, equipotential lines, and flow rate, is obtained by selecting the Groundwater calculation option. In solving Finite Elements, 6656 triangular elements and 3449 nodes are used. The equipotential lines drawn by the Finite Element Method in the Partial Differential Equation Toolbox are shown in Figure 3.

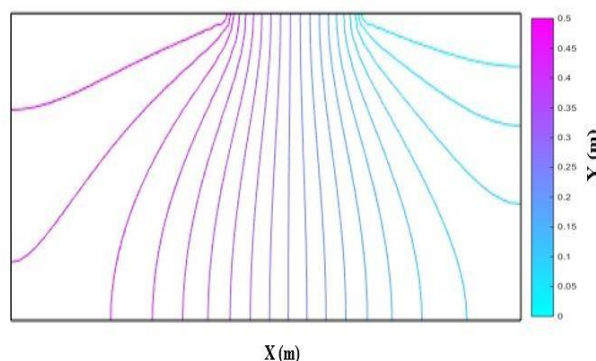


Fig. 3: Finite element method of equipotential lines

One of the critical features of the RBF meshless method is the possibility of solving the problem with very few points as an initial approximation. The problem of Figure 2 is solved once by considering 6 points, of which 3 points are



inside the computational area and 3 points are on the borders, and then the number of points is increased to 15 (12 border points, 3 inside points), 28 (18 border points, 10 inside points), 45 (24 border points, 21 inside points), 91 (36 border points, 55 inside points) and 133 (48 border points, 85 inside points) points and the results were evaluated. By adopting different values for  $\alpha$ , the matrices of  $c$  are obtained, and then by selecting  $\alpha$  or the same optimal shape factor through validation, the water head can be obtained at any desired point. The error diagram of the RBF method compared to the Finite Element Method is shown in Figure 4.

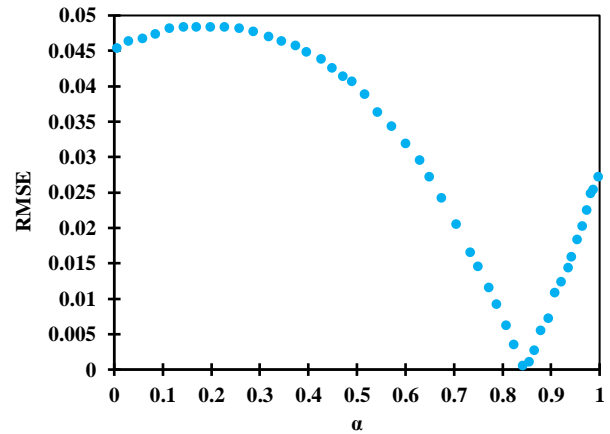


Fig. 4: RBF method error compared to Finite Element Method for different shapes factors ( $\alpha$ ).

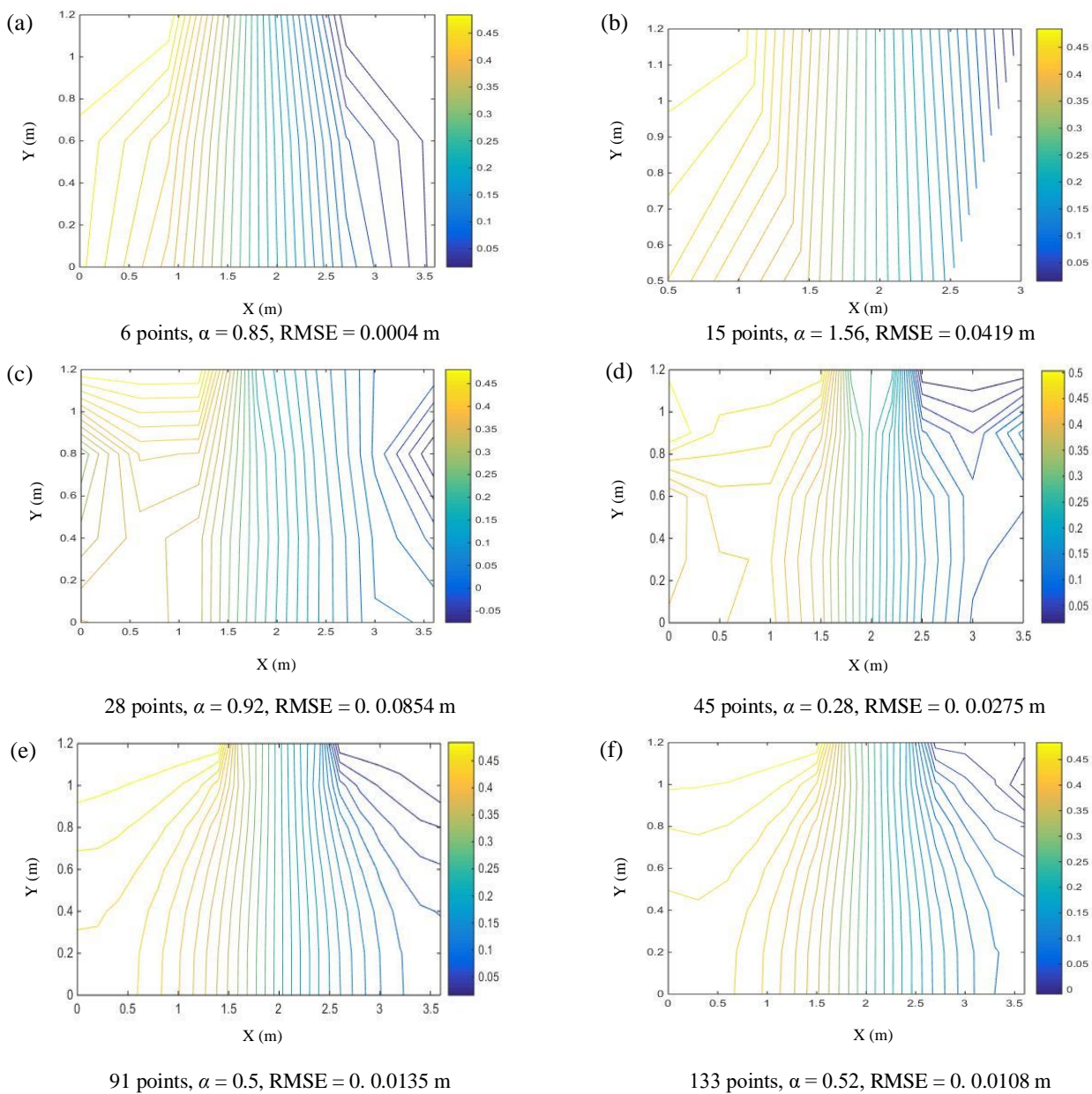


Fig. 5: Equipotential lines below the dam with an increasing number of points.

For  $\alpha = 0.85$ , the calculation error is minimized by 6 points compared to the Finite Element Method. Similarly, the optimal shape factor for all points was found, and the equipotential lines below the dam were drawn in Figure 5 respectively.

It can be seen that considering the 6 points, the general shape of all drawn equipotential lines is not suitable despite having a small error, and the potential lines are not perpendicular to the boundaries. On the other hand, the dimensions of the computational area are not covered. The equipotential lines below the dam must correspond to the shape of the lines drawn by the Finite Element Method. The RMSE obtained in problem-solving with 6 points is close to zero, but the shape of the contours is not appropriate. Therefore, it can be said that the number of 6 points cannot indicate the geometry of the computational area because the dimensions of the computational area are 3.6 meters by 1.2 meters, but these dimensions are not covered. Therefore, it can be concluded that the low calculation error is not enough to investigate the problem of seepage under the dam, so the problem has no hydraulic justification, and the number of points needs to be increased. This step is done only as an initial approximation and finding a range of shape factors.

In the next step, the number of points is increased to 15. It is observed that the geometry of the computational area is determined according to the problem statement, but the equipotential lines below the dam are not similar to the equipotential lines provided by the Finite Element Method. By selecting 28 points, it was observed that the dimensions of the computational area are covered, but the shape of the equipotential lines below the dam does not match the lines of equipotential provided by the Finite Element Method. Also, contrary to reality, negative values have been obtained for the water head. On the other hand, verticality is not seen on all impenetrable boundaries. Therefore, the number of points must be increased for good hydraulic compliance. By increasing the number of points to 45 points, it is observed that the dimensions of the computational area are covered. The error has decreased from 0.0854 in the previous step to 0.0275 at this step.

On the other hand, the shape of the contours under the dam and the perpendicularity to the impermeable borders have also improved compared to the previous step. Therefore, it can be said that problem-solving is converging and reaching the desired state. With increasing the number of points to 91 points, it is observed that the equipotential lines below the dam have high compliance, and the dimensions of the computational area are covered. At this step, the error has decreased from 0.0275 in the previous step to 0.0135. By increasing the number of points to 133 points, the lines of equipotential under the dam are matched with the lines of equipotential under the dam by the Finite Element Method, and the dimensions of the computational area are covered.

Comparing the error of the obtained results with the Finite Element Method shows a downward trend in the last 4 steps. This trend indicates the convergence of the problem and reaching the correct answer. The calculation error is minimized compared to the finite element method for 6 points so that the root mean square error (RMSE) for 6 points is 0.0004 meters, and this value is 0.0108 meters for 133 points. From the most important results of Figure 5, we can point out the basic case that having appropriate statistical values such as RMSE is not enough to investigate the problem, and the hydraulics governing the problem (equipotential lines) must be investigated. In general, we can say that by increasing the number of points, the accuracy of solving the problem increases, and the shape factor converges to a number. On the other hand, with increasing points, the ability to draw equipotential lines under the dam increases. In Table 1, to validate, some points in the area of solution and boundaries are randomly selected, and the water head in these points is presented using the RBF method and Finite Element after calculation.

**Table 1:** Comparison results of the RBF method with the FEM method in a steady flow

x (m)	y (m)	RBF (m)	FEM (m)	AE (m)	RMSE (m)	RRMSE (%)	R <sup>2</sup>
0.8	0.7	0.4478	0.4496	0.0018			
1.2	1	0.4559	0.4588	0.0029			
2.6	0.55	0.1320	0.1344	0.0024	0.0028	1.146	0.9995
0	0.9	0.4825	0.4807	0.0018			
2.2	0	0.2476	0.2526	0.005			
1	0.2	0.4056	0.4071	0.0015			

The x and y columns represent the coordinates of the selected points, third and fourth columns represent the water head obtained by RBF and FEM methods, respectively. The proximity of absolute error, root mean square error, and relative root mean square error to zero and coefficient of determination to 1 indicates the conformity of the RBF numerical solution method with the Finite Element Method. After investigating the seepage in the steady state, the transient state was considered by increasing the upstream head. In the case of the study by Hashemi and Hatam [15], the head of water increases linearly from 0.5 m to 1.5 m for 300 minutes, as shown in Figure 6.

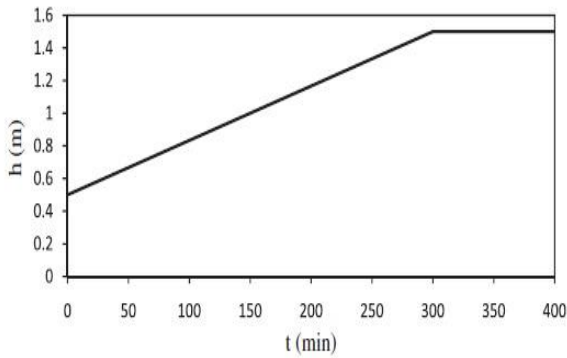


Fig. 6: Water head increase upstream of the dam during 300 min [15].

The finite difference was used to discretize time statements, and the RBF method was used for spatial statements to solve the equation in transient flow. First, the shape factor was calibrated for the transient state, and then the equipotential lines below the dam for different periods were plotted according to Figure 7.

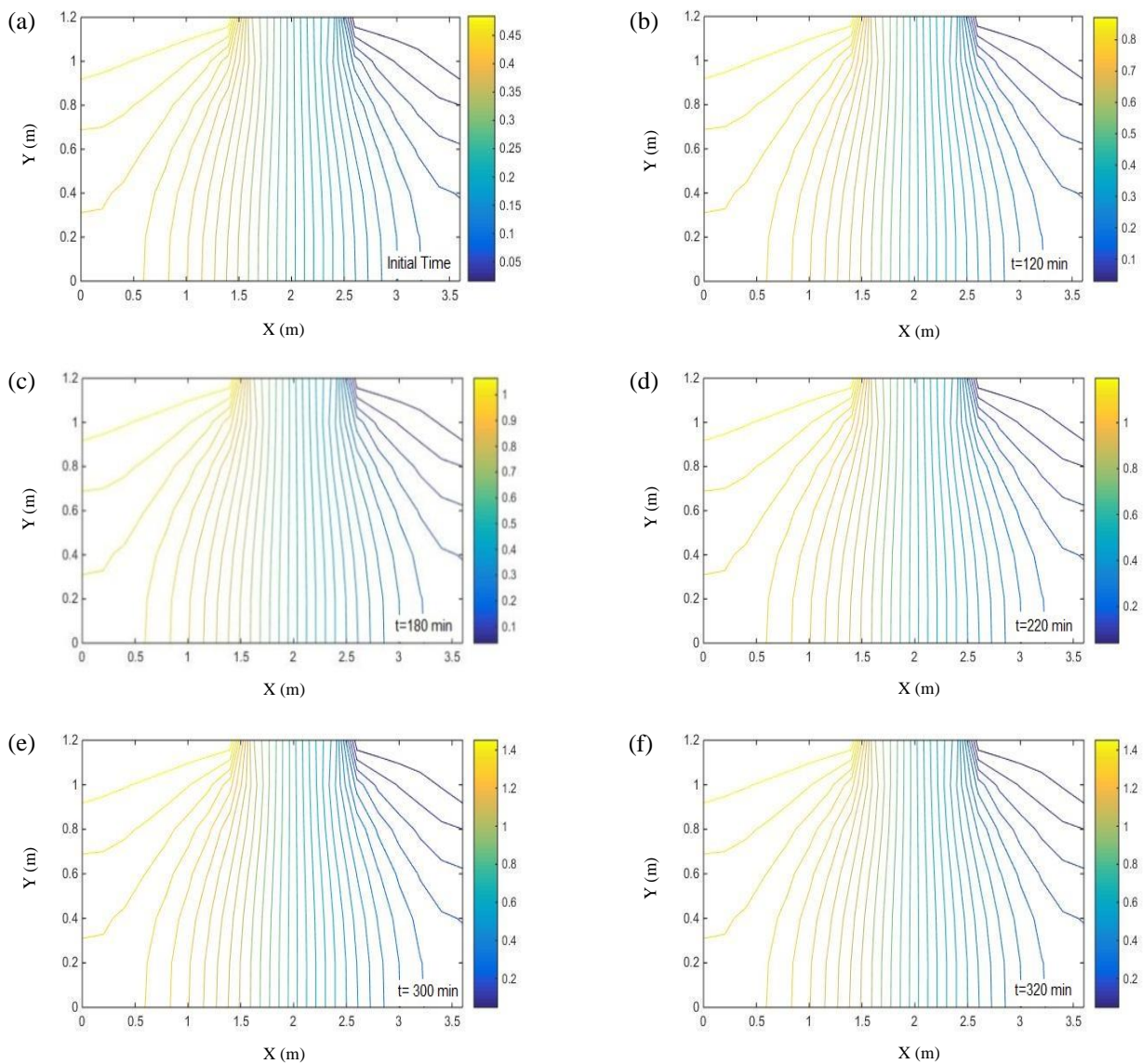


Fig. 7: Head contours in different time steps by RBF method.

At 120 minutes, after starting to increase the depth, the water head upstream increases by 0.4 m and reaches 0.9 m. Following the increase of the upstream water head, the water

head of the points within the computational area increases. At 300 minutes after starting to increase the upstream water head, it increases by 1 meter and reaches 1.5 meters.



Therefore, the water head of the points inside the computational area increases. During this period, the general shape of the contour has remained constant at different times. The increase of the head is completed in 300 minutes. At 320 minutes, the upstream water head is fixed at 1 m. The equipotential lines below the dam at 320 minutes are similar to those below at 300 minutes. This similarity indicates that the flow has returned to a steady state after 300 minutes. Several points from the solution area and boundaries were randomly selected at different time intervals to validate the results. The water head at these points is shown in Tables 2 and 3 using the RBF method, finite element, and Local RBF-

DQ. The proximity of AE, RMSE, and RRMSE statistical indicators to zero and  $R^2$  to 1 indicate the conformity of the RBF method with the finite element method. In the study of transient flow, a calibrated coefficient for the steady state was used. The consistency of the results in Tables 2 and 3 shows that applying the calibrated shape factor in the steady flow can be used in the transient flow. This finding indicates that the shape factor in the RBF method is independent of the flow mode and depends on the geometry and the governing differential equation.

**Table 2:** Comparison of the water head results of the RBF method with FEM in the transient state

x (m)	y (m)	Time (min)	RBF (m)	FEM (m)	AE (m)	RMSE (m)	RRMSE (%)	$R^2$
1	0	0	0.41	0.41	0.004	0.00912	1.078	0.9994
		120	0.72	0.71	0.01			
		180	0.88	0.89	0.01			
		240	1.05	1.06	0.01			
		300	1.20	1.19	0.01			
2	0	0	0.25	0.25	0.004	0.00663	1.274	0.9985
		120	0.45	0.45	0.002			
		180	0.55	0.56	0.01			
		240	0.65	0.66	0.01			
		300	0.75	0.75	0.0001			

**Table 3:** Comparison of the water head results of the RBF method with Local RBF\_DQ in the non-steady state

x (m)	y (m)	Time (min)	RBF (m)	Local RBF-DQ (m)	AE (m)	RMSE (m)	RRMSE (%)	$R^2$
2	0.6	0	0.25	0.26	0.005	0.0045	1.0756	0.9992
		120	0.45	0.45	0.002			
		180	0.55	0.55	0.003			
		220	0.61	0.62	0.007			
		300	0.75	0.75	0.004			
3	1	0	0.031	0.031	0.0025	0.0012	1.7709	0.996
		120	0.054	0.055	0.001			
		180	0.064	0.069	0.002			
		220	0.075	0.076	0.001			
		300	0.09	0.091	0.001			

#### 4. Conclusions

For the steady flow condition:

1- To primarily solve the problems and get a good approximation of the answers, the above method can be used

by using several points inside the solution area and several points on the borders. This study considered 3 points at the Dirichlet and 3 points at the Newman boundary conditions

as a preliminary approximation. In the initial approximation, the shape factor was 0.85, and RMSE was equal to 0.0004.

2- It was observed that the results obtained from applying several points for solving have no hydraulic justification and are insufficient to draw equipotential below the dam despite having a low error.

3- The initial approximations of the shape factor are close to the original answer.

4- By solving the problem and calibrating the value of the shape factor, the amount of water head can be obtained at any desired point.

For transient flow condition:

1- Similar to the steady state, geometry, and boundaries must be determined through a series of points to draw equipotential lines.

2- Since the shape factor of the base function depends on the geometry and the governing equation, the same shape factor was used for the steady and transient state. The verification performed, and the consistency of the results with the results of previous studies confirm the mentioned issue.

3- By increasing the upstream water head of the dam from 0.5 meters to 1.5 meters, the water head in the points below the dam also increases. However, after the water level behind the dam remains constant, the water head below the dam also reaches a constant value.

## Acknowledgments

The authors of this article would like to thank all those who accompanied us in writing this article.

## Notation

The following symbols are used in this paper:

$B$  = differential operators at the interior points

$C_i$  = unknown coefficients

$h$  = hydraulic head

$h_D$  = water head upstream of the concrete dam

$h_U$  = water head downstream of the concrete dam

$h_{FEM}$  = water head in the Finite Element Method

$h_{RBF}$  = water head in the RBF meshless method

$k_x$  = hydraulic conductivity in the direction of  $x$

$k_y$  = hydraulic conductivity in the direction of  $y$

$k_r$  = relative permeability

$L$  = differential operators at the boundary points

$N$  = total number of nodes

$n$  = porosity

$P$  = pressure head

$r$  = distance between points

$RBF$  = Radial Basis Function

$S_s$  = special maintenance

$S_w$  = water saturation ratio

$\alpha, \beta, n$  = values obtained by calibration

$\phi_i$  = shape function

## References

- [1] Huang, T., Rudnicki, J. W., A. (2006). Mathematical model for seepage of deeply buried groundwater under higher pressure and temperature. *Journal of hydrology*, 327 (1-2), 42-54.
- [2] Honjo, Y., Giao, P. H., & Naushahi, P. A. (1995). Seepage analysis of Tarbela dam (Pakistan) using finite element method. *International Journal of Rock Mechanics and Mining Sciences and Geomechanics Abstracts*, 32 (3), 131A.
- [3] Brebbia, C. A., Chang, O. V. (1979). Boundary elements applied to seepage problems in zoned anisotropic soils, *Advances in Engineering Software*, 1 (3), 95-105.
- [4] Darbandi, M., Torabi, S. O., Saadat, M., Daghighi, Y., & Jarrabashi, D. (2007). A moving-mesh finite volume method to solve free-surface seepage problem in arbitrary geometries. *Numerical and analytical methods in Geomechanics*, (31) 41, 1609-1629.
- [5] Daneshfaraz, R., Kaya, K. (2008). Solution of the propagation of the waves in open channels by the transfer matrix method. *Ocean Engineering*, 35 (11-12), 1075-1079.
- [6] Abbaszadeh, H., Norouzi, R., Sume, V., Kuriqi, A., Daneshfaraz, R., & Abraham, J. (2023). Sill Role Effect on the Flow Characteristics (Experimental and Regression Model Analytical). *Fluids*, 8(8), 235.
- [7] Daneshfaraz, R., Norouzi, R., Abbaszadeh, H., Kuriqi, A., & Di Francesco, S. (2022). Influence of sill on the hydraulic regime in sluice gates: an experimental and numerical analysis. *Fluids*, 7(7), 244.
- [8] Li, J., Chen, Y., & Pepper, D. (2003). Radial basis function method for 1D and 2D groundwater contaminant transport modeling. *Computational Mechanics*, 32 (1-2), 10-15.
- [9] Gingold, R. A., Monaghan, J. J. (1977). Smoothed particle hydrodynamics: theory and application to non-spherical stars. *Monthly notices of the royal astronomical society*, 181 (3), 375-389.
- [10] Kansa, E. (1990). Multiquadrics-A scattered data approximation scheme with application to computational fluid dynamics. Solution to parabolic, hyperbolic and elliptic partial differential equations. *Computers & Mathematics with Applications*, 19 (8-9), 147-161.
- [11] Boztosun, I., Charafi, A., Zerroukat, M., & Djidjeli, K. (2002). Thin-plate spline radial basis function scheme for advection-diffusion problems. *Electric Journal of Boundary Elements*, 2, 889-895.
- [12] Sarler, B., Perko, J., & Chen, C.S. (2004). Radial basis function collocation method solution of natural convection in porous media. *International Journal of Numerical Methods for Heat & Fluid Flow*, (14)2, 187-212.

- [13] Durmus, A., Boztosun, I., & Yasuk, F. (2006). Comparative study of the multiquadratic and thin-plate spline radial basis function for the transient-convection diffusion problem. *International Journal of Modern Physics C.*, (17)8, 1151-1169.
- [14] Nourani, V., Mousavi, Sh. (2016). Spatiotemporal groundwater level modeling using hybrid artificial intelligence-meshless method. *Journal of Hydrology*, 536, 10-25.
- [15] Hashemi, M. R., Hatam, F. (2011). Unsteady seepage analysis using local radial basis function-based differential quadrature method. *Applied Mathematical Modeling*, 35, 4934-4950.
- [16] Ouria, A., Toufigh, M. M., & Nakhani, A. (2007). An investigation on the effect of the coupled and uncoupled formulation on transient seepage by the finite element method. *American Journal of Applied Sciences*, (4)12, 950-956.
- [17] Cooley, R. L. (1983). Some new procedures for numerical solution of variably saturated flow problems. *Water Resources Research*, (19)5, 1271-1285.
- [18] Bear, J., Verruijt, A. (1987). Modeling Two-Dimensional Flow in Aquifers. In: Modeling Groundwater Flow and Pollution. Theory and Applications of Transport in Porous Media, vol 2. Springer, Dordrecht, [https://doi.org/10.1007/978-94-009-3379-8\\_4](https://doi.org/10.1007/978-94-009-3379-8_4)
- [19] Das, B. M., Sobhan, K. (2013). *Principles of geotechnical engineering*. Cengage Learning.
- [20] Daneshfaraz, R., Abbaszadeh, H., Gorbanvatan, P., & Abdi, M. (2021). Application of Sluice Gate in Different Positions and Its Effect on Hydraulic Parameters in Free-Flow Conditions. *Journal of Hydraulic Structures*, 7(3), 72-87.
- [21] Daneshfaraz, R., Norouzi, R., Abbaszadeh, H., & Azamathulla, H. M. (2022). Theoretical and experimental analysis of applicability of sill with different widths on the gate discharge coefficients. *Water Supply*, 22(10), 7767-7781.
- [22] Hassanzadeh, Y., & Abbaszadeh, H. (2023). Investigating Discharge Coefficient of Slide Gate-Sill Combination Using Expert Soft Computing Models. *Journal of Hydraulic Structures*, 9(1), 63-80.
- [23] Daneshfaraz, R., Norouzi, R., & Abbaszadeh, H. (2022). Experimental investigation of hydraulic parameters of flow in sluice gates with different openings. *Environment and Water Engineering*, 8(4), 923-939.



This article is an open-access article distributed under the terms and conditions of the Creative Commons Attribution (CC-BY) license.